

Supporting Information

High-Performance BiVO₄ Photoanodes: Elucidating the Combined Effects of Mo-Doping and Modification with Cobalt Polyoxometalate

Fan Feng,^a Dariusz Mitoraj,^b Ruihao Gong,^c Dandan Gao,^a Mohamed M. Elnagar,^b
Rongji Liu,^a Radim Beranek,^{b,*} Carsten Streb^{a,*}

^a Department of Chemistry, Johannes Gutenberg University Mainz, Duesbergweg 10-14,
55128 Mainz, Germany

^b Institute of Electrochemistry, Ulm University, Albert-Einstein-Allee 47, 89081 Ulm, Germany

^c Institute of Inorganic Chemistry I, Ulm University, Albert-Einstein-Allee 11, 89081 Ulm,
Germany

* Corresponding authors: radim.beranek@uni-ulm.de, carsten.streb@uni-mainz.de

1. Experimental Section

Materials: Fluorine-doped tin oxide (FTO) Pilkington TEC glass was purchased from XOP company (XOP Glass, Castellón Spain). Sodium hydroxide (NaOH, $\geq 99\%$) was provided by Carl Roth GmbH & Co. KG. Boric acid (H_3BO_3 , 99.5%), cobalt (II) nitrate hexahydrate ($\text{Co}(\text{NO}_3)_2 \cdot 6\text{H}_2\text{O}$, 98%), bismuth (III) nitrate pentahydrate ($\text{Bi}(\text{NO}_3)_3 \cdot 5\text{H}_2\text{O}$, $\geq 98.0\%$), ethylene glycol ($\text{C}_2\text{H}_6\text{O}_2$, $\geq 99\%$), polyethyleneimine (PEI, 50 wt%, dissolved in water), tri-block copolymer F-108 and bis(acetylacetonate) dioxomolybdenum (VI) ($\text{MoO}_2(\text{acac})_2$) were all supplied by Sigma-Aldrich. Sodium tungstate dihydrate ($\text{NaWO}_4 \cdot 2\text{H}_2\text{O}$) and hydrochloric acid (HCl, 37%) were provided by Merck. Sodium sulfite (Na_2SO_3 , 98%) and ammonia solution (NH_4OH , 25%) were purchased from J.T. Baker. Potassium dihydrogen phosphate (KH_2PO_4 , 99.0%) was purchased from Applichem GmbH. Sodium chloride (NaCl, 99%) was provided by abcr GmbH & Co. KG. Potassium phosphate (K_2HPO_4 , 99+%), glacial acetic acid (CH_3COOH , 99.5%), sodium phosphate (Na_2HPO_4 , 99+%) and vanadyl (IV) acetylacetonate ($\text{C}_{10}\text{H}_{14}\text{O}_5\text{V}$, 99%) were obtained from Acros Organics.

Preparation of Mo-BiVO₄ substrates: Mo-BiVO₄ photoanodes were deposited on cleaned FTO by a spin-coating process.¹ In a typical synthesis procedure, 0.15 M $\text{Bi}(\text{NO}_3)_3 \cdot 5\text{H}_2\text{O}$ as Bi precursor was dissolved in the solvent containing 1.5 mL ethylene glycol, 2 mL glacial acetic acid and 0.5 mL deionized water at room temperature. After stirring for 15 min, 0.3 M $\text{VO}(\text{acac})_2$ as V precursor was added subsequently to the above solution, stirred for another 1 h. Then 240 μL of 50 mM $\text{MoO}_2(\text{acac})_2$ ethylene glycol solution as a doping element was added to the above solution. The 0.35 g F-108 as a structural agent was then added in and stirred for 2 h to make a porous structure. After that, a uniform viscous ink for spin coating was obtained. Mo-BiVO₄ photoanodes were deposited on cleaned FTO-coated glass substrates at 50 rps for 30 s followed by drying at 250 °C for 5 min and the above coating and drying process was repeated five times. Finally, samples were calcined in a muffle oven at 450 °C for 1 hour with a heating rate of 3 °C/min. After sintering, 1 M NaOH was used to remove the excess V_2O_5 . Pristine BiVO₄ was obtained by the same procedure omitting the addition of the Mo-precursor. Mo-BiVO₄(500 °C) and Mo-

BiVO_4 (400 °C) was obtained by the same procedure except calcined temperature. $\text{Mo}(400 \mu\text{L})\text{-BiVO}_4$ and $\text{Mo}(80 \mu\text{L})\text{-BiVO}_4$ was obtained by the same procedure except adding 400 μL and 80 μL of $\text{MoO}_2(\text{acac})_2$ ethylene glycol solution into precursor solution, respectively.

Synthesis of CoPOM: The CoPOM complex was synthesized according to literature.² Briefly, $\text{NaWO}_4 \cdot 2\text{H}_2\text{O}$ (35.62 g, 0.108 mol), $\text{Na}_2\text{HPO}_4 \cdot 7\text{H}_2\text{O}$ (1.70 g, 0.012 mol) and $\text{Co}(\text{NO}_3)_2 \cdot 6\text{H}_2\text{O}$ (6.98 g, 0.024 mol) were dissolved in 100 mL deionized water in a 200 mL round-bottom flask. After adjusting the pH to 7 by 9 M HCl under magnetic stirring, this purple suspension was then stirred and refluxed at 105°C for 2 hours. After reflux, the solution was saturated with 36 g NaCl and allowed to cool to room temperature. The resulting purple crystals were collected, quickly washed with approximately 30 mL of water, and recrystallized from hot water. The identity of the CoPOM is confirmed by Fourier transform infrared spectroscopy (FT-IR).

Preparation of Mo-BiVO₄/CoPOM: The Mo-BiVO₄ electrode was dipped into the aqueous CoPOM (5 mM) solution for 5 min, then rinsed with distilled water and dried in air. Then this process was repeated 5 times to acquire the desired amount of CoPOM and the sample was named as Mo-BiVO₄/CoPOM. Repeating 3 times (Mo-BiVO₄/CoPOM 3L), 5 times (Mo-BiVO₄/CoPOM 5L) and 8 times (Mo-BiVO₄/CoPOM 8L) were obtained by choosing different times of impregnation.

Preparation of Mo-BiVO₄/PEI+CoPOM: The Mo-BiVO₄ modified with PEI and CoPOM was prepared by dipping the Mo-BiVO₄ electrode into an aqueous PEI (6 mM) solutions of sodium phosphate (10 mM, pH = 5.4~5.7) and NaCl (137 mM) for 5 min, then rinsed with distilled water and dried in air, followed by dipping in CoPOM solution (5 mM) for another 5 min. The dipping processes in PEI and CoPOM solution were repeated 5 times and named as Mo-BiVO₄/PEI+CoPOM.³

Preparation of Mo-BiVO₄/CoPi: CoPi was loaded on Mo-BiVO₄ via the photo-assisted electrodeposition method previously reported.⁴ Briefly, the electrolyte is 0.5 mM $\text{Co}(\text{NO}_3)_2$ dissolved in 0.1 M sodium phosphate buffer solution with pH value of 7.0. The prepared Mo-BiVO₄ photoanode was taken as the working electrode, Pt as the counter electrode and Ag/AgCl as the reference electrode (3.5 M KCl),

respectively. The photo-assisted electrodeposition was conducted at a bias of 0.4 V vs. Ag/AgCl (1.0 V vs. RHE) for 1 min under simulated sunlight (AM1.5G at 100 mW cm⁻²).

Preparation of Mo-BiVO₄/CoO(OH)_x: Loading with CoO(OH)_x nanoparticles in Mo-BiVO₄ photoanodes was using a two-step impregnation process.⁵ First, the prepared Mo-BiVO₄ photoanodes were immersed into an aqueous solution of 0.1 M Co(NO₃)₂ for 10 minutes at room temperature. Subsequently, the electrodes were dried in air, quickly dipped into NH₄OH solution and dried again in air.

Characterization: The *UV-vis absorption spectra* were determined by a UV-Vis spectrophotometer (UV-2600, Shimadzu, Japan) equipped with the integrating sphere. The absorbance (Abs.) was calculated by the equation:

$$\text{Absorbance (\%)} = 100\% - \text{Reflectance (\%)} - \text{Transmittance (\%)}$$

The baselines were recorded using an FTO glass and a BaSO₄ plate as references for transmittance and reflectance, respectively (Fig. S5a). Scanning Electron Microscopy (SEM) and energy-dispersive X-ray spectroscopy (EDX) elemental mapping of samples before the PEC operation were performed using a ZEISS LEO 1550 VP scanning electron microscope operating at an acceleration voltage of 15 kV and coupled with energy dispersive spectroscopy (EDS, Ametek, USA). To improve the conductivity and achieve higher resolution SEM imaging and EDS analysis for the cross-sectional view, a 10 nm thick layer of C was deposited onto the sample surface. The EDX mappings of samples after the PEC operation were recorded with an AMETEK EDAX Octane Elite detector (the used software was APEX in version 2.5.1001.0001), and a 15nm thick carbon layer was deposited for better conductivity. For the focused ion beam (FIB) cross sections, a Zeiss NVision 40 Ar was used. For better-cut quality, the region of interest was treated with a felt tip pen (Pilot Super Color Marker). The at% of C is subtracted for the presented values in the EDS analysis of the cross-sectional view. Transmission electron microscopy (TEM) and energy-dispersive X-ray spectroscopy (EDX) elemental mapping were recorded with FEI Tecnai G2 Spirit. *Fourier transform infrared spectroscopy (FT-IR)* was performed on a Bruker Tensor 27 equipped with a PIKE Miracle Diamond ATR unit. *X-ray photoelectron spectroscopy (XPS)* measurements were performed with monochromatized Al K α radiation (250 W, 15 kV) using a PHI 5800 ESCA system.

The binding energies were calibrated based on C 1s peak of adventitious carbon (284.8 eV). *X-ray diffraction (XRD)* patterns were recorded on a Rigaku XRD-6000 diffractometer under the following conditions: 40 kV, 40 mA, CuK α radiation ($\lambda = 0.154$ nm). Inductively coupled plasma atomic emission spectrometry (ICP-AES) was performed on a Perkin Elmer Plasma 400 spectrometer.

Photoelectrochemical measurements: The photoelectrochemical measurements were conducted using a SP-300 BioLogic potentiostat in a typical 3-electrode system with a Pt wire as counter electrode, an Ag/AgCl (3.5 M KCl, 0.205 V vs. SHE) as reference electrode and film photoanodes as working electrodes with geometric irradiation area of 0.5 cm². A 150 W Xe lamp (L.O.T.-Oriol) was employed as the light source with a light power density of 100 mW cm⁻², equipped with a KG-3 (LOT-Quantum Design) heat-absorbing filter and an AM 1.5G filter. All electrodes were illuminated from back-side (through FTO glass).

All potentials of photoelectrodes in this paper are reported against RHE:⁶

$$E_{RHE} = E_{Ag/AgCl} + 0.205 + 0.059 \times pH$$

where E_{RHE} is the converted potential referred to the RHE and $E_{Ag/AgCl}$ is the experimentally measured potential against the Ag/AgCl reference electrode.

The charge separation efficiency (η_{sep}) and the hole transfer efficiency (η_{tr}) were calculated for the prepared photoanodes using the approach reported by Donat et al.⁷

The hole transfer efficiency (η_{tr}) was determined using the equation:

$$\eta_{tr} = \frac{J_{H_2O}}{J_{Na_2SO_3}}$$

where J_{H_2O} and $J_{Na_2SO_3}$ are the photocurrents measured in the absence and presence of an additional hole scavenger (Na₂SO₃, 0.1 M) which is a readily oxidizable reducing agent.

The charge separation efficiency (η_{sep}) is estimated by the equation:

$$\eta_{sep} = \frac{J_{Na_2SO_3}}{J_{max}}$$

where J_{max} is the maximal photocurrent density obtained by integrating the absorbance spectrum (Fig. S5b) over the AM 1.5G solar spectrum from 300 nm to 560 nm with absorbance.

The incident photon-to-current conversion efficiency (IPCE) was recorded using a photoelectric spectrometer (Instytut Fotonowy Sp. z o.o.) equipped with a 150 W Xenon lamp and a monochromator, according to the equation:¹

$$IPCE(\%) = \frac{1240J_{ph}}{\lambda P} 100\%$$

where J_{ph} is the photocurrent density under monochromatic light, P is the monochromatic light power density, λ is the irradiation wavelength.

The applied bias photoconversion efficiency (ABPE) was also used to quantify the photoanode performance following the below equation:⁸

$$ABPE(\%) = \frac{J_{ph}(1.23 - V_{app})}{P} 100\%$$

in which J_{ph} is the photocurrent density, V_{app} is the applied bias (V vs. RHE), and P is the incident light density (100 mW cm⁻²).

The oxygen evolution was recorded by the FireSting optical fiber oxygen meter (PyroScience, GmbH) in a home-made air-tight two-compartment cell using a Pt working electrode with the oxygen collection efficiency as approximately 50.2% ± 3.8%, which is value as a standard faradaic efficiency (FE, only based on dissolved O₂), 100.0% ± 7.6%. The volume of the photoanode compartment was 4.6 mL. The electrolyte was bubbled with argon before the electrodes were illuminated under an applied potential of 0.74 V vs. RHE. The electrolyte was 0.5 M aqueous sodium borate buffer electrolyte with a pH value of 9.0.

2. Analytical section

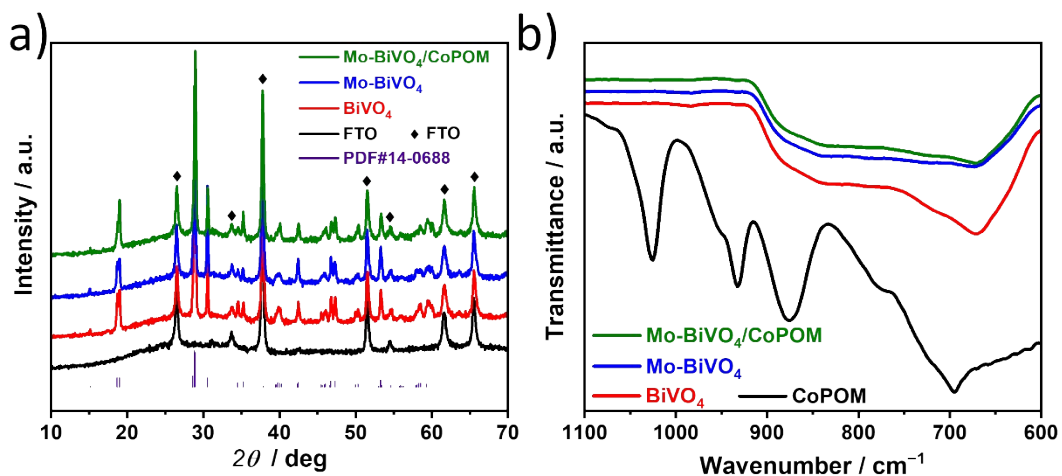
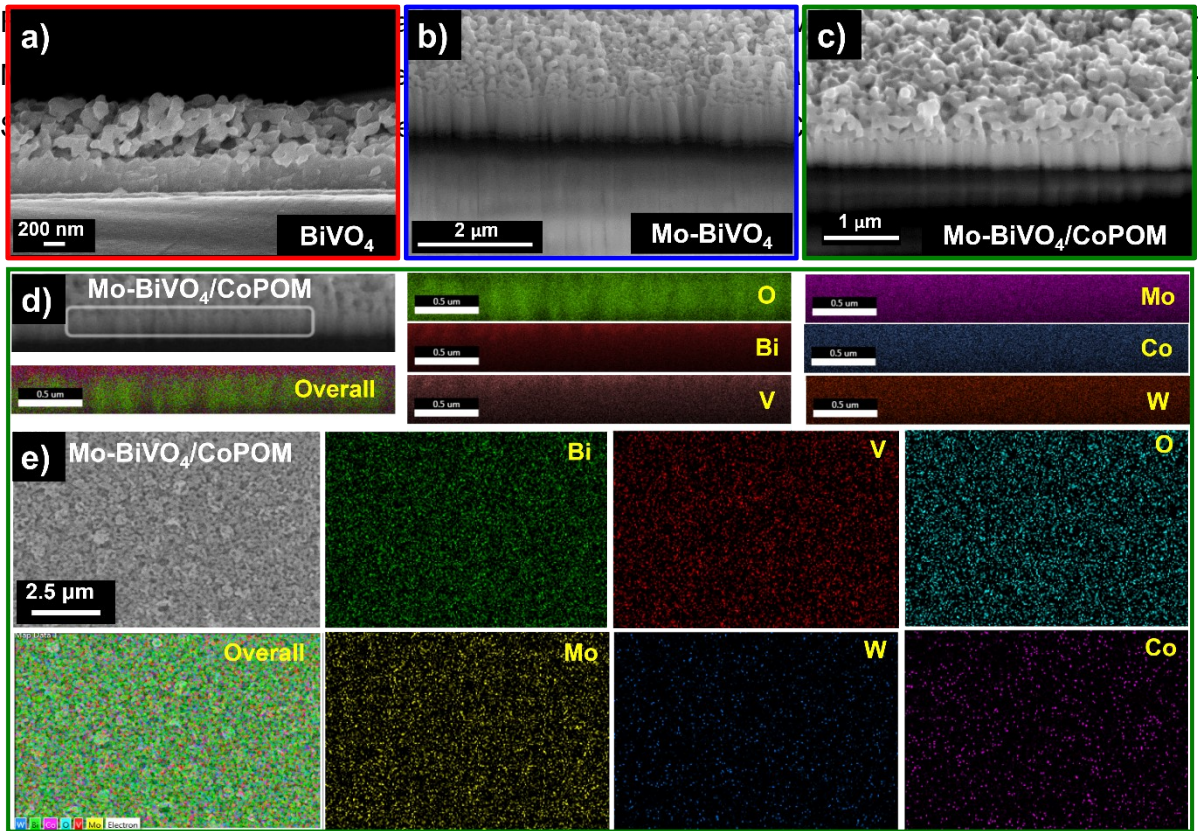


Fig. S1 (a) XRD patterns of BiVO₄, Mo-BiVO₄, Mo-BiVO₄/CoPOM and FTO substrate. Asterisk denotes reflections of the FTO substrate. Vertical lines represent the literature⁹ pattern of bismuth vanadate (PDF # 14-0688) and (b) ATR-FTIR spectra of all BiVO₄-containing photoanodes and CoPOM powder.



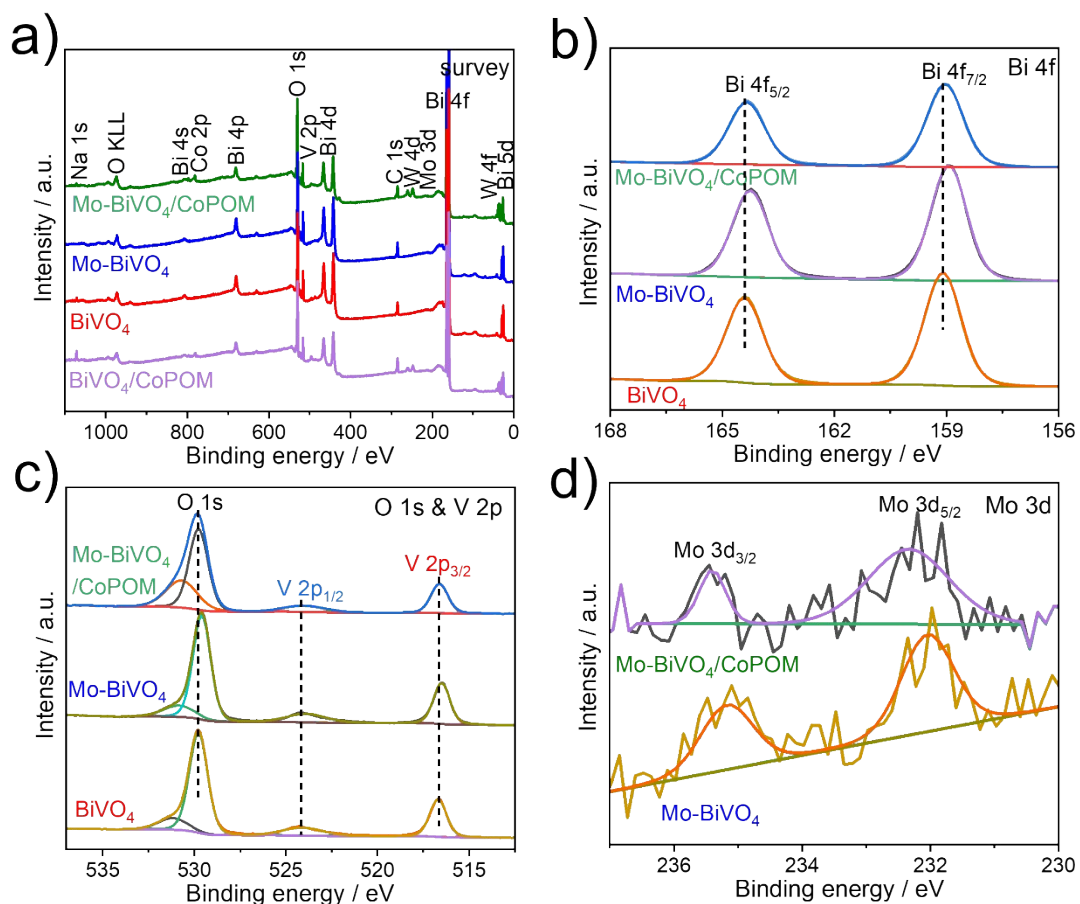


Fig. S3 (a) XPS survey spectra of BiVO₄, Mo-BiVO₄, Mo-BiVO₄/CoPOM and BiVO₄/CoPOM. (b) Bi 4f and (c) O1s and V 2p XPS spectra of BiVO₄, Mo-BiVO₄ and Mo-BiVO₄/CoPOM photoanodes. (d) Mo 3d XPS spectra of Mo-BiVO₄, Mo-BiVO₄/CoPOM photoanodes.

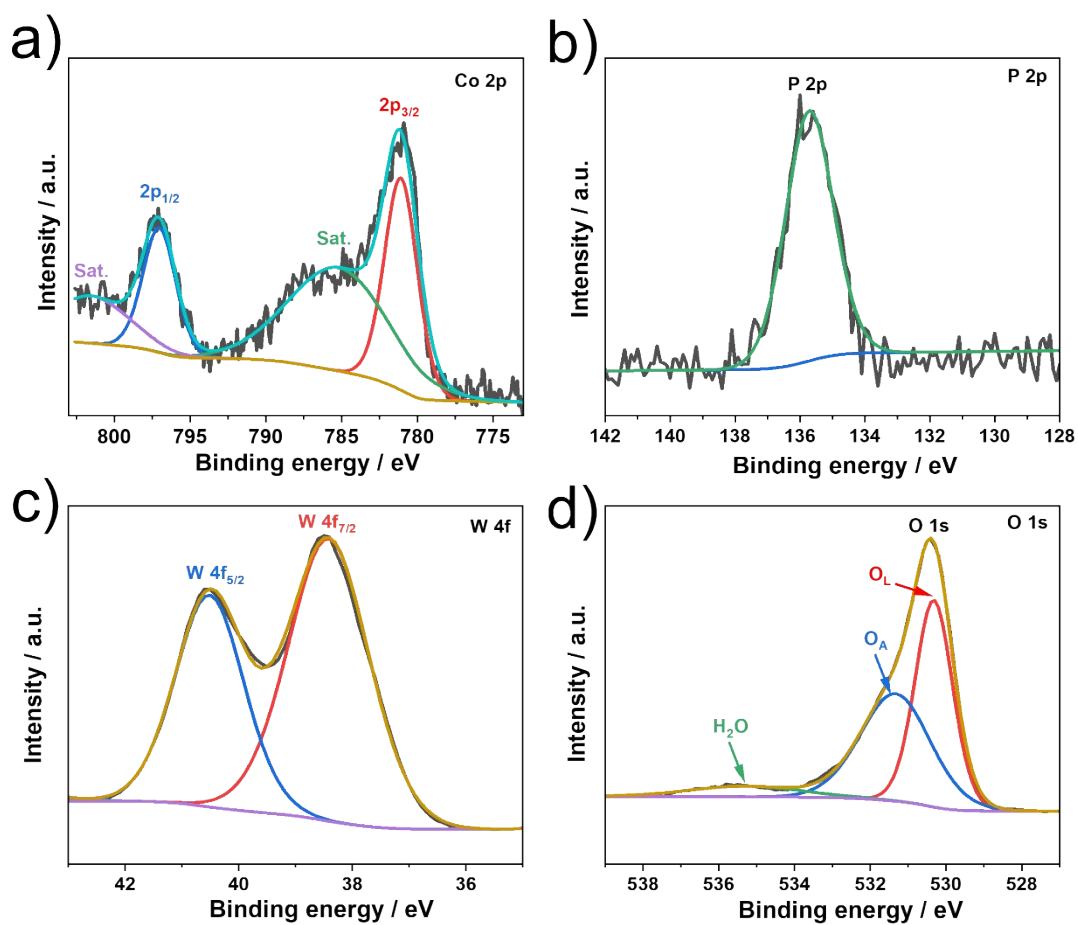


Fig. S4 XPS spectra of **CoPOM powder** (a) Co 2p, (b) P 2p, (c) W 4f and (d) O 1s.

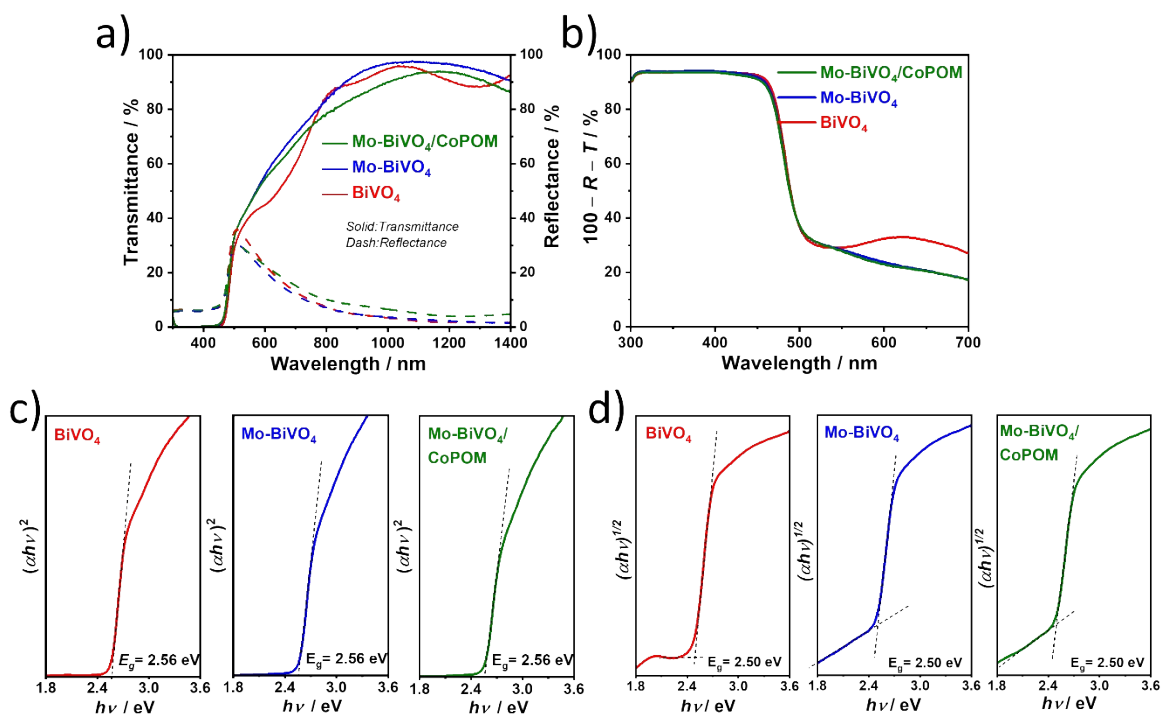


Fig. S5 (a, b) UV-Vis electronic absorption spectra of the photoanodes. $Absorbance$ (%) = $100\% - Reflectance$ (%) - $Transmittance$ (%). The nonzero baseline can be ascribed to the differences in internal reflection and scattering at the FTO/ BiVO_4 interface in the transmittance and reflectance measurement modes.¹⁰ Determination of the fundamental optical absorption edge using the Tauc approach for direct (c) and indirect (d) bandgaps.

Tab. S1 Concentrations (in at.%) of elements detected by SEM-EDX.

| Samples | Bi | V | Mo | W | Co | O |
|-----------------------------|-----------|----------|-----------|----------|-----------|----------|
| Mo-BiVO ₄ /CoPOM | 15.27 | 13.51 | 0.79 | 1.92 | 0.95 | 67.59 |
| Mo-BiVO ₄ | 15.22 | 15.14 | 1.16 | - | - | 68.49 |
| BiVO ₄ | 16.27 | 16.23 | - | - | - | 67.50 |

Tab. S2 Concentrations (in at.%) of elements detected by XPS.

| Samples | C | Na | Bi | V | Mo | W | Co | O |
|-----------------------------|----------|-----------|-----------|----------|-----------|----------|-----------|----------|
| BiVO ₄ | 18.9 | 1.6 | 18.4 | 8.1 | - | - | - | 53.1 |
| Mo-BiVO ₄ | 21.0 | - | 17.7 | 8.3 | 0.1 | - | - | 52.9 |
| Mo-BiVO ₄ /CoPOM | 19.6 | 0.9 | 12.3 | 6.0 | 0.1 | 3.1 | 2.3 | 55.8 |

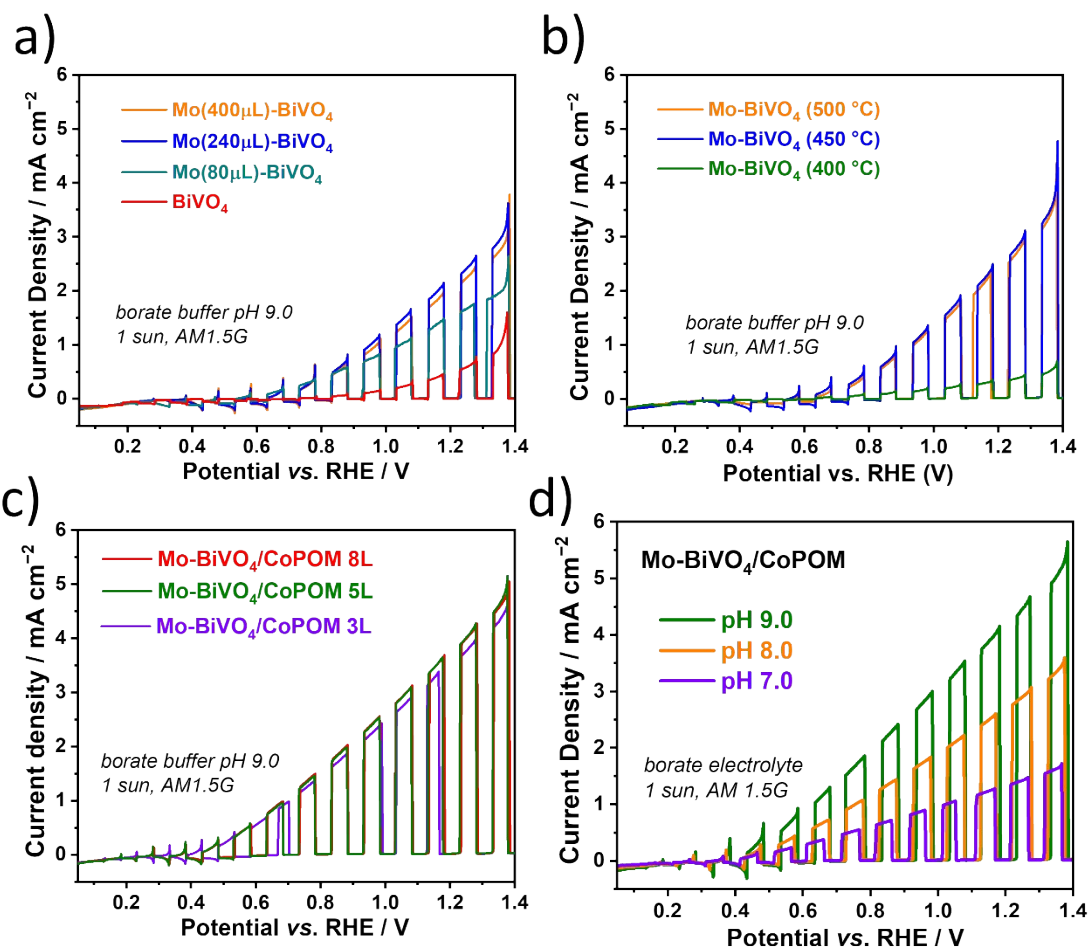


Fig. S6 *J-V* curves of (a) different amounts for Mo doping on BiVO_4 photoanodes, (b) different temperatures for calcination of Mo-BiVO_4 photoanodes, (c) different amounts for CoPOM on Mo-BiVO_4 photoanodes measured in sodium borate buffer electrolyte (pH = 9.0) under AM 1.5G one sun and (d) different pH for sodium borate electrolyte for $\text{Mo-BiVO}_4/\text{CoPOM}$ photoanodes measured under AM 1.5G (1 sun).

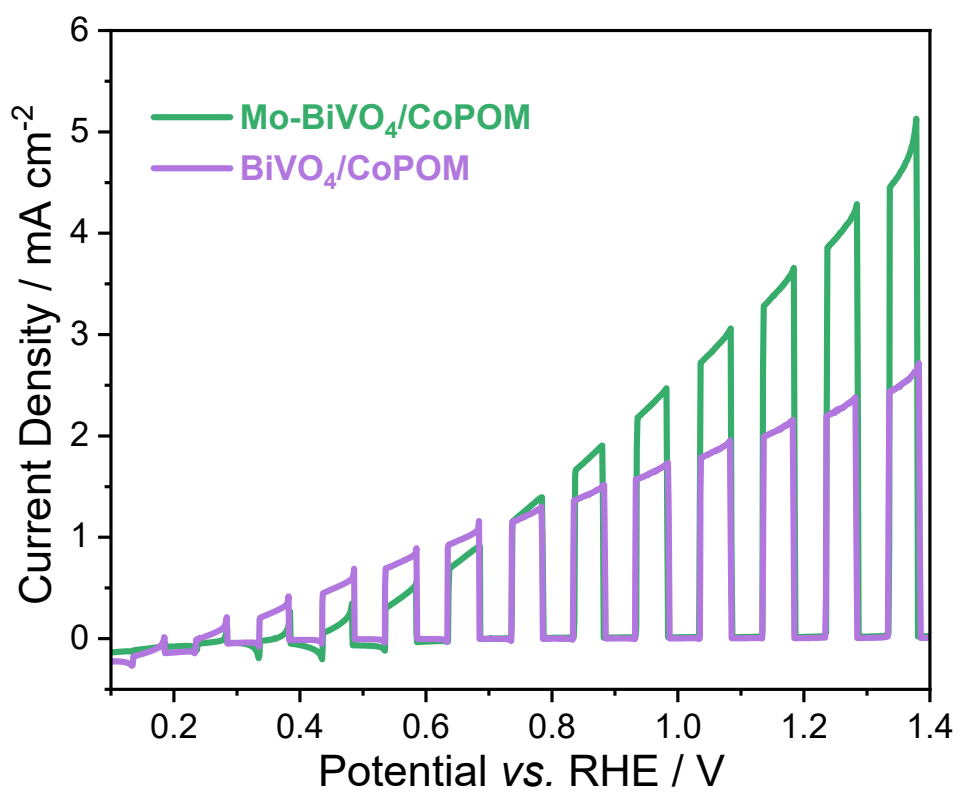


Fig. S7 Photocurrents recorded under AM 1.5G (1 sun) illumination in a borate electrolyte (0.5 M, pH 9.0) for Mo-BiVO₄/CoPOM and BiVO₄/CoPOM.

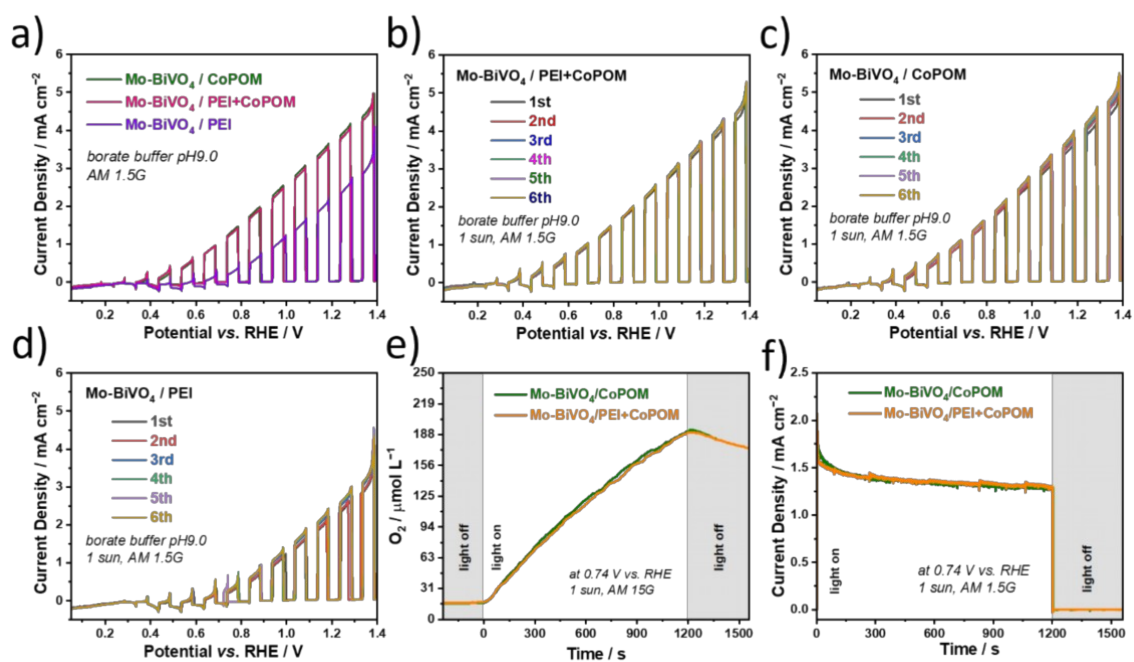


Fig. S8 J - V curves of (a) Mo-BiVO₄ with CoPOM, PEI or PEI+CoPOM; Photocurrent stability test recorded under AM 1.5G illumination at cathodic sweep of 10 mV s⁻¹ for (b) Mo-BiVO₄/PEI+CoPOM, (c) Mo-BiVO₄/CoPOM and (d) Mo-BiVO₄/PEI. (e) Dioxygen evolution and (f) corresponding photocurrent transients.

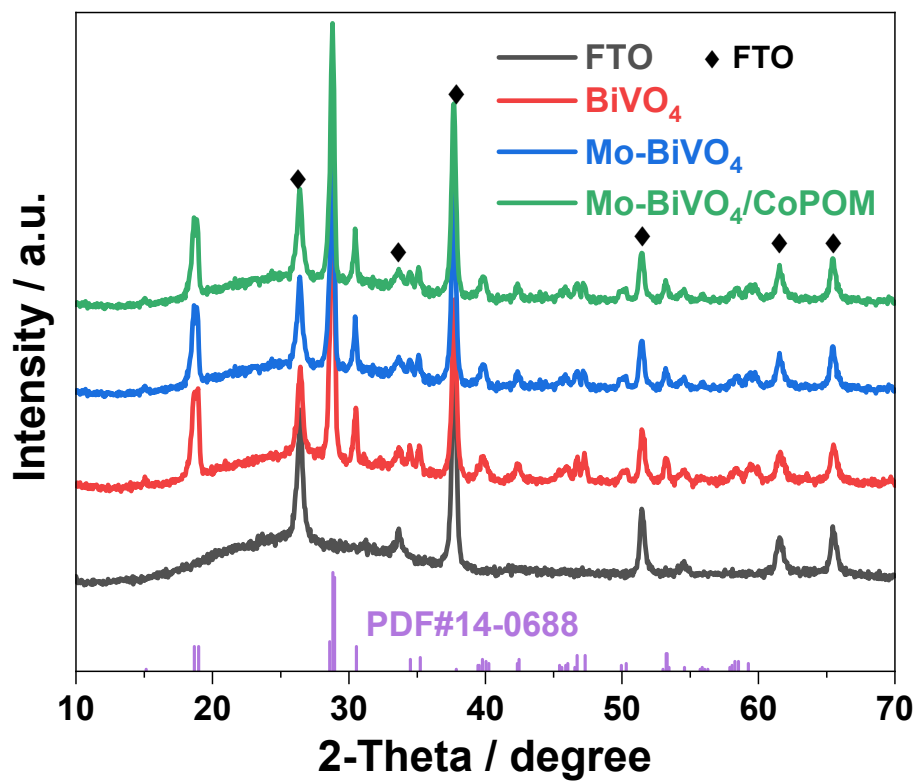
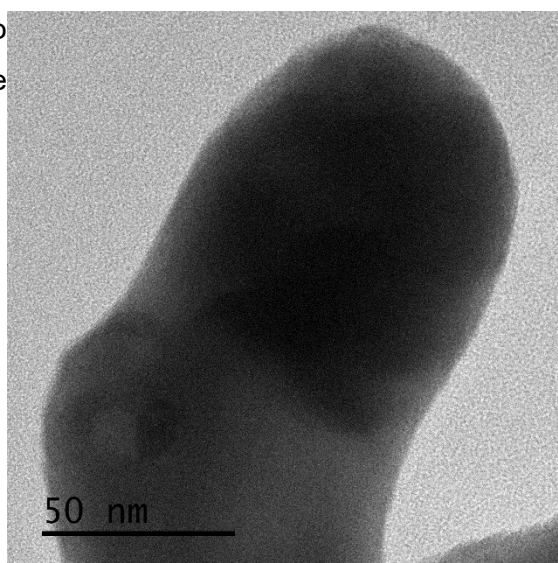


Fig. S9 XRD patterns of BiVO_4 , Mo-BiVO_4 , $\text{Mo-BiVO}_4/\text{CoPOM}$ after PEC for 4 h in borate buffer electrolyte (0.5 M, pH 9.0) at 0.74 V vs. RHE and FTO substrate.

Fig. S10 High-resolution TEM image of $\text{Mo-BiVO}_4/\text{CoPOM}$ after PEC operation for 4 h in borate buffer electrolyte.



PEC operation for 4 h in borate buffer electrolyte

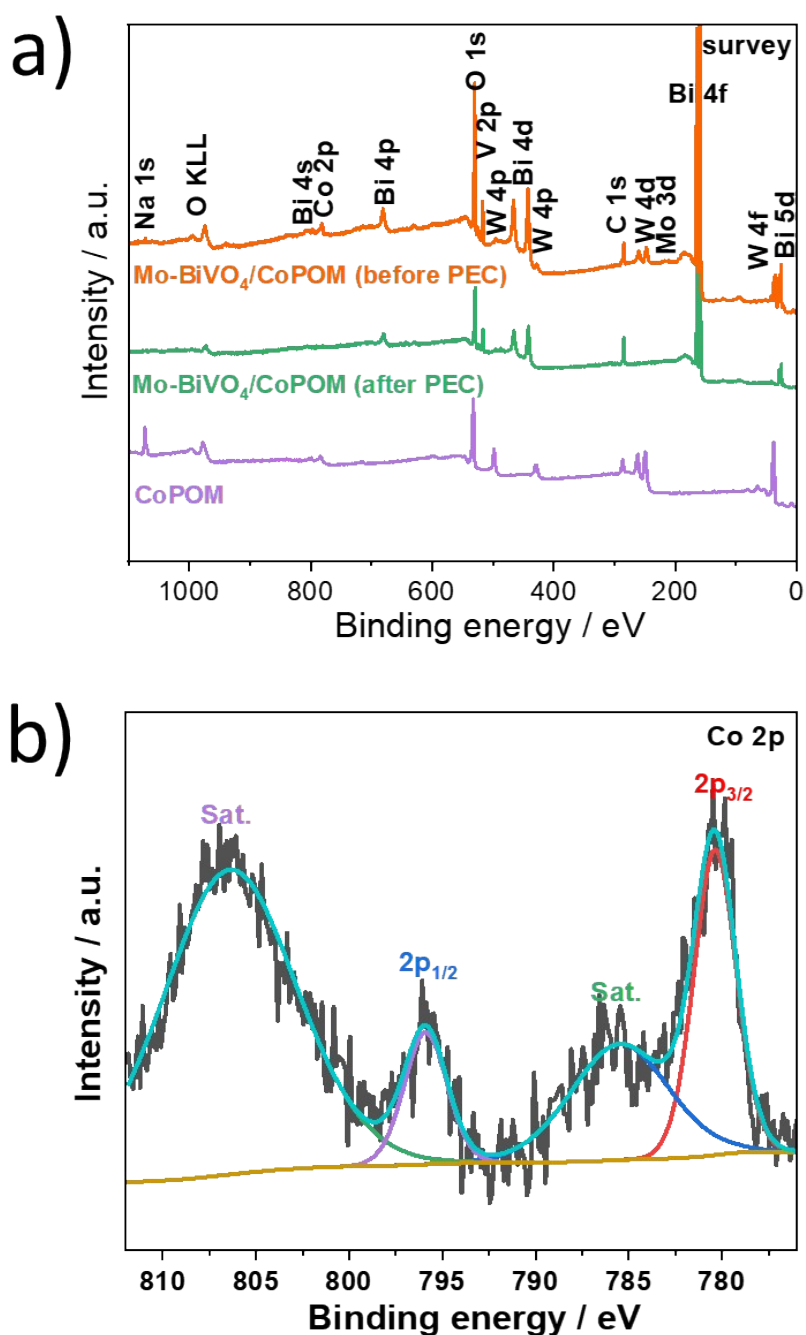


Fig. S11 (a) XPS survey spectra of CoPOM powder, Mo-BiVO₄/CoPOM photoanodes *before* and *after PEC* for 4 h in borate buffer electrolyte (0.5 M, pH 9.0) at 0.74 V vs. RHE. (b) High resolution XPS spectra of Co 2p for Mo-BiVO₄/CoPOM photoanodes *after PEC* for 4 h in borate buffer electrolyte (0.5 M, pH 9.0) at 0.74 V vs. RHE.

Tab. S3 Concentrations (in at.%) of elements detected by XPS for Mo-BiVO₄/CoPOM measured before and after the PEC experiment for 4 h in borate buffer electrolyte (0.5 M, pH 9.0) at 0.74 V vs. RHE.

| Samples | C | Na | Bi | V | Mo | W | Co | O | Ratio (W/Co) |
|----------------|----------|-----------|-----------|----------|-----------|----------|-----------|----------|---------------------|
| Before | 19.6 | 0.9 | 12.3 | 6.0 | 0.1 | 3.1 | 2.3 | 55.8 | 1.3 |
| After | 38.4 | 0.0 | 12.2 | 6.8 | 0.0 | 0.4 | 0.2 | 42.0 | 2.0 |

Tab. S4 Concentration (in at.%) of the detected elements in SEM-EDX (from the top-view) for Mo-BiVO₄/CoPOM measured before and after PEC experiment for 4 h in borate buffer electrolyte (0.5 M, pH 9.0) at 0.74 V vs. RHE.

| Samples | Bi | V | Mo | W | Co | O | Ratio (W/Co) |
|----------------|-----------|----------|-----------|----------|-----------|----------|---------------------|
| Before | 15.27 | 13.51 | 0.79 | 1.92 | 0.95 | 67.59 | 2.1 |
| After | 10.45 | 9.41 | 0.91 | 3.79 | 0.25 | 75.19 | 15.2 |

Tab. S5 Concentration (in at.%) of the detected W and Co by SEM-EDX (from the cross-sectional view) for Mo-BiVO₄/CoPOM measured before and after PEC experiment for 4 h in borate buffer electrolyte (0.5 M, pH 9.0) at 0.74 V vs. RHE.

| Samples | W | Co | Ratio (W/Co) |
|----------------|----------|-----------|---------------------|
| Before | 0.64 | 0.41 | 1.56 |
| After | 0.80 | 0.21 | 3.81 |

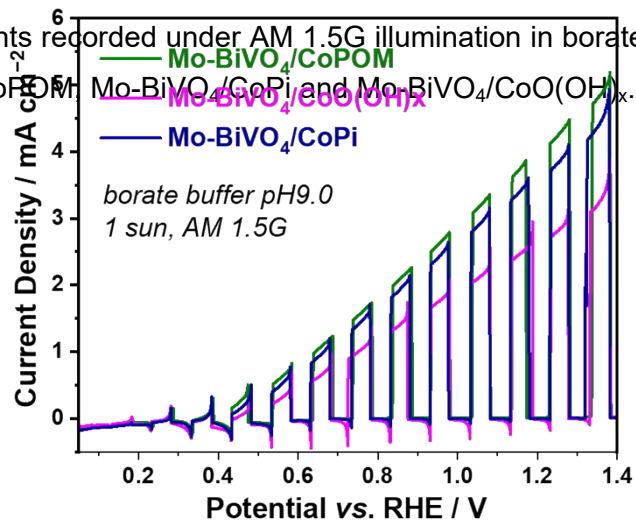
Tab. S6 ICP-AES of cobalt measured in the electrolyte before and after chronoamperometry at 0.74 V vs. RHE under AM 1.5G one sun illumination for a Mo-BiVO₄/CoPOM electrode.

| Probe | Element | Result | Unit | Stand. deviation | Unit |
|---|---------|--------------|------|------------------|------|
| 1 – Pristine borate buffer solution | Co | not detected | | | |
| | K | 1,5422 | mg/L | 0,3600 | % |
| | Na | 3351,3333 | mg/L | 3,8156 | % |
| | P | not detected | | | |
| | W | 0,0956 | mg/L | 0,0378 | % |
| | B | 3458,0000 | mg/L | 2,5699 | % |
| 2 – Borate buffer solution after PEC experiment | Co | not detected | | | |
| | K | 7,8625 | mg/L | 0,3625 | % |
| | Na | 3076,5000 | mg/L | 2,6358 | % |
| | P | 0,6363 | mg/L | 0,0038 | % |
| | W | 0,0688 | mg/L | 0,0063 | % |
| | B | 3196,5000 | mg/L | 3,5699 | % |
| 3 – Pristine phosphate buffer solution | Co | not detected | | | |
| | K | 38146,0000 | mg/L | 4,5699 | % |
| | Na | 83,6600 | mg/L | 0,7500 | % |
| | P | 15634,0000 | mg/L | 3,6330 | % |
| | W | 0,2550 | mg/L | 0,1025 | % |
| | B | 5,2790 | mg/L | 0,4138 | % |
| 4 – Phosphate buffer solution after PEC experiment | Co | not detected | | | |
| | K | 38620,0000 | mg/L | 3,2319 | % |
| | Na | 85,8600 | mg/L | 4,8500 | % |
| | P | 16122,0000 | mg/L | 3,1255 | % |
| | W | 0,1250 | mg/L | 0,0125 | % |
| | B | 3,8528 | mg/L | 0,3625 | % |

Tab. S7. Photoelectrochemical performance (photocurrent density at 1.23 V vs. RHE and maximum ABPE) of selected BiVO₄-based photoanodes from the literature.

| References | Photoanodes | Electrolyte | Photocurrent (1.23 V _{RHE}) | ABPE (maximum) |
|-------------------|--|--|--|-------------------|
| 3 ^{ref} | FeNiPO _x /BiVO ₄ | 0.5 M K ₃ BO ₃ | 6.73 mA cm ⁻² | ~2.3% |
| 20 ^{ref} | Gradient W:BiVO ₄ /CoPi | 0.1 M KPi | 3.6 mA cm ⁻² | Not reported |
| 21 ^{ref} | BiVO ₄ /FeOOH/NiOOH | 0.5 M KPi | 4.2 mA cm ⁻² | 1.75% |
| 24 ^{ref} | BiVO ₄ -85/Co-Pi | 0.5 M KPi | 2.94 mA cm ⁻² | Not reported |
| 27 ^{ref} | CoBi/E-BiVO ₄ | 1 M KBi | 3.2 mA cm ⁻² | 1.1% |
| 29 ^{ref} | BiV _{0.97} Mo _{0.03} O ₄ /FeOOH | 0.1 M KPi | 3.0 mA cm ⁻² | Not reported |
| 30 ^{ref} | WO ₃ /Mo-BiVO ₄ /Co-Pi | 0.1 M KPi | 2.4 mA cm ⁻² | Not reported |
| 35 ^{ref} | Mo:BiVO ₄ -NiFeO _x | 0.5 M Na ₂ SO ₄ | ~1.2 mA cm ⁻² | Not reported |
| 37 ^{ref} | Co-Pi/BiV _{0.98} Mo _{0.02} O ₄ | 0.5 M Na ₂ SO ₄ | ~1 mA cm ⁻² | Not reported |
| 38 ^{ref} | BiVO ₄ /CoPi | 0.5 M K ₂ SO ₄ + 0.09 M KH ₂ PO ₄ + 0.01 M K ₂ HPO ₄ | 1.7 mA cm ⁻² | Not reported |
| 40 ^{ref} | N-BiVO ₄ /NiFeO _x | 0.5 M K ₃ BO ₃ | 5.40 mA cm ⁻² | 1.79% |
| 41 ^{ref} | BiVO ₄ /Au/NiFeOOH | 0.5 M K ₃ BO ₃ | 5.3 mA cm ⁻² | 1.56% |
| 42 ^{ref} | BiVO ₄ /NiCo ₂ S ₄ | 0.5 M Na ₂ SO ₄ | 1.4 mA cm ⁻² | Not reported |
| 56 ^{ref} | BiVO ₄ -(b-PEI/POM) ₁₀ | 80 mM KPi | ~2.8 mA cm ⁻² | Not reported |
| 58 ^{ref} | BiVO ₄ -N/C-CoPOM | 0.5 M KPi | 3.30 mA cm ⁻² | 1.22% |
| 59 ^{ref} | La:BaSnO ₃ -Mo:BiVO ₄ | 1 M KPi | 3.23 mA cm ⁻² | Not reported |
| S11 ¹¹ | BiVO ₄ /ZnFe ₂ O ₄ /Bi NPs | 0.5 M Na ₂ SO ₄ | 2.72 mA cm ⁻² | 0.51% |
| S12 ¹² | Ni:FeOOH/BiVO ₄ | 0.5 M Na ₂ SO ₄ | 4.21 mA cm ⁻² | 0.80% |
| S13 ¹³ | -0.8 V reduced- BiVO ₄ /FeOOH | 0.2 M Na ₂ SO ₄ | 2.02 mA cm ⁻² | 0.51% |
| S14 ¹⁴ | NiFeV/B-BiVO ₄ | 1 M KBi | 4.6 mA cm ⁻² | 1.85% |
| This work | Mo-BiVO ₄ /CoPOM | 0.5 M KBi | 4.32 mA cm ⁻² | 0.73% |

Fig. S12 Photocurrents recorded under AM 1.5G illumination in borate electrolyte (0.5 M, pH 9.0) for Mo-BiVO₄/CoPOM, Mo-BiVO₄/Co(OH)_x, Mo-BiVO₄/CoPi and Mo-BiVO₄/CoO(OH)_x.



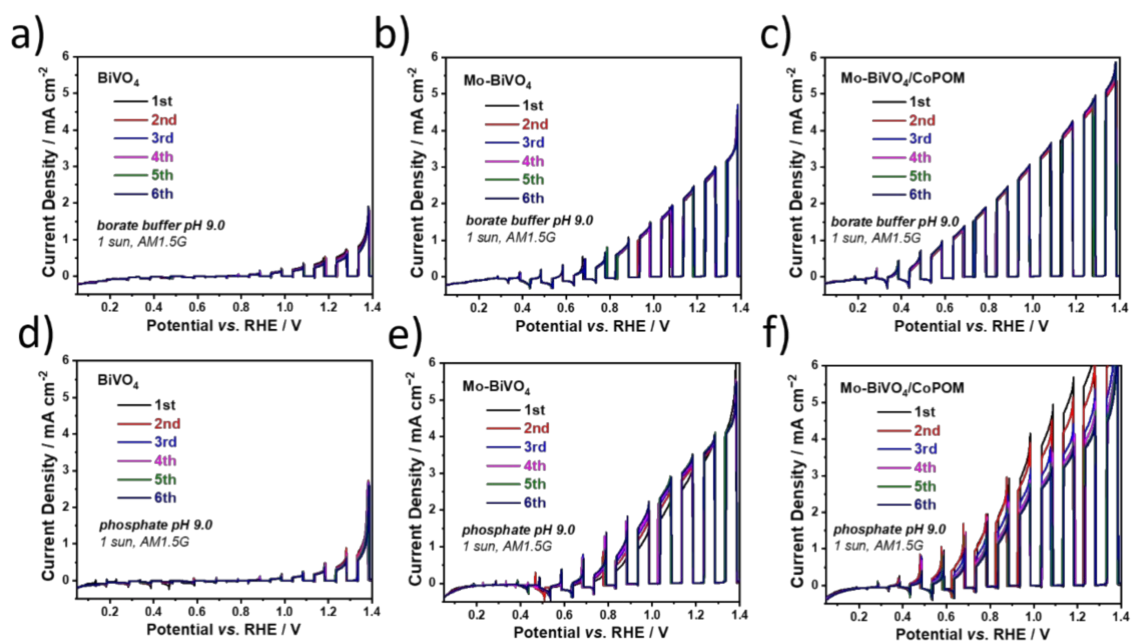


Fig. S13 Photocurrent stability test recorded under AM 1.5G one sun illumination at cathodic sweep of 10 mV s⁻¹ for three photoanodes in (a-c) a borate buffer electrolyte of pH value 9.0 and (d-f) a phosphate electrolyte of pH value 9.0.

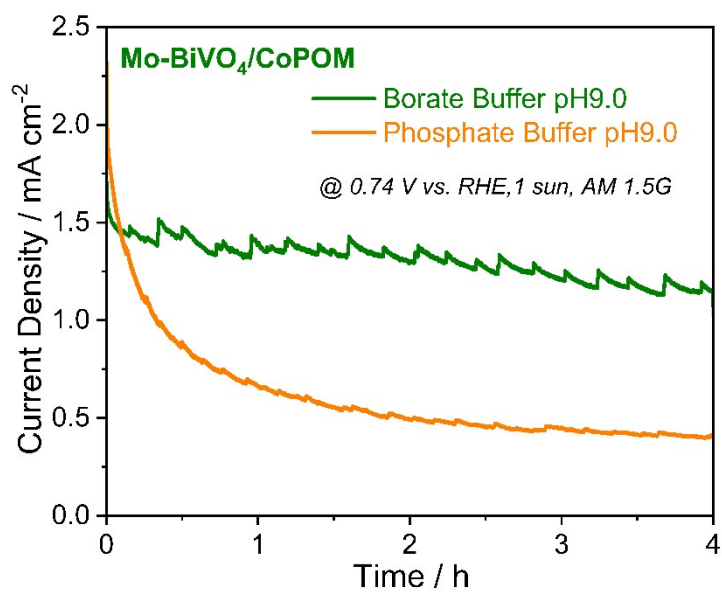


Fig. S14 Stability chronoamperometry curves for Mo-BiVO₄/CoPOM in borate buffer (0.5 M, pH 9.0) and phosphate electrolyte (0.5 M, pH 9.0) at 0.74 V vs. RHE under AM 1.5G (1 sun) illumination.

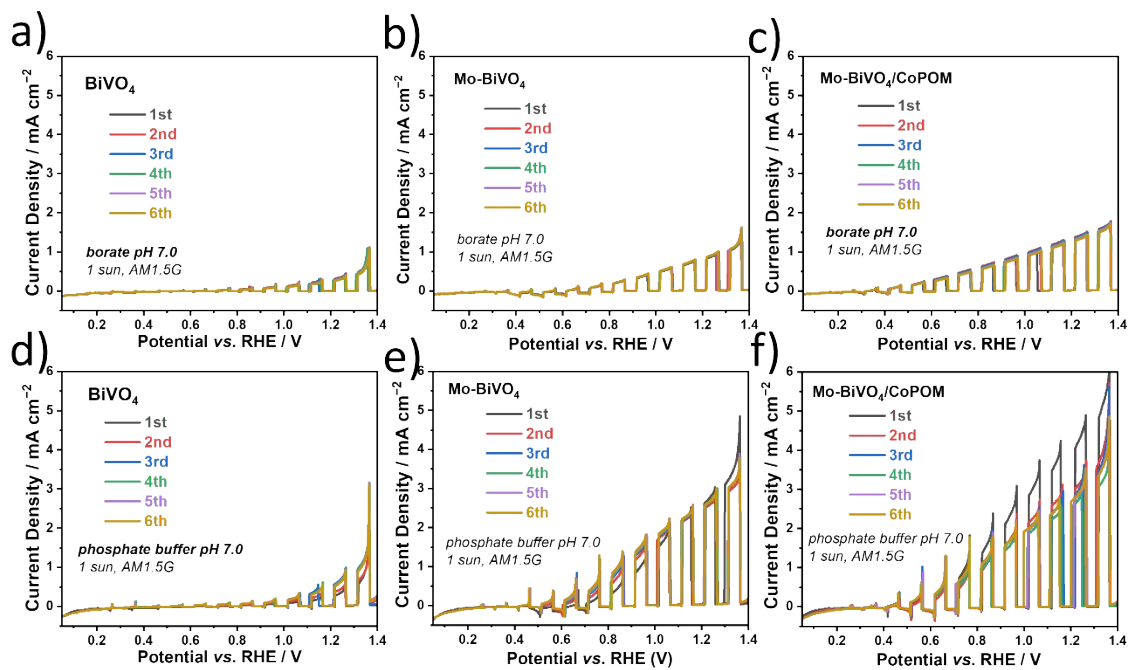
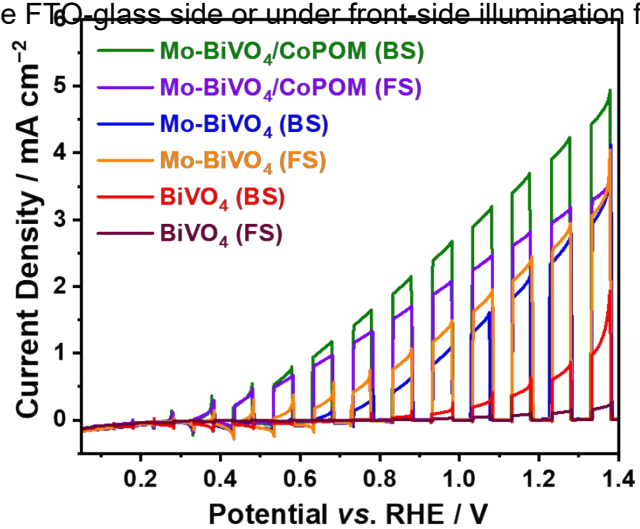


Fig. S15 Photocurrent stability test recorded under AM 1.5G illumination at cathodic sweep of 10 mV s⁻¹ for three photoanodes in (a-c) a borate buffer electrolyte of pH value 7.0 and (d-f) a phosphate buffer electrolyte of pH value 7.0.

Fig. S16 *J-V* curves under AM 1.5G one sun illumination for all three photoanodes under back-side illumination from the FTO glass side or under front-side illumination from the active layer material side.



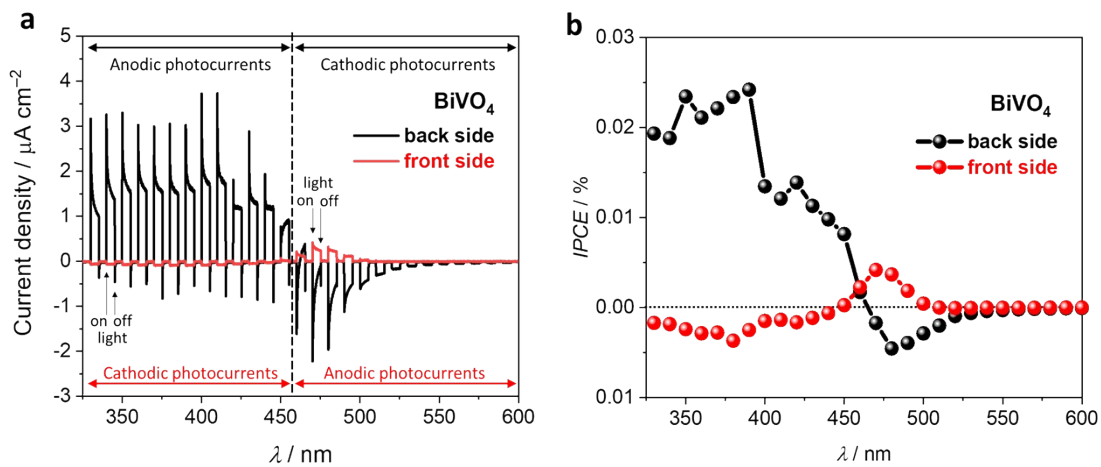


Fig. S17 Photocurrent transients (a) and the corresponding IPCE spectra (b) measured at a pristine BiVO₄ photoanode under the front-side and back-side chopped irradiation with monochromatic light of different wavelengths in borate electrolyte (pH 9.0) at 0.74 V vs. RHE.

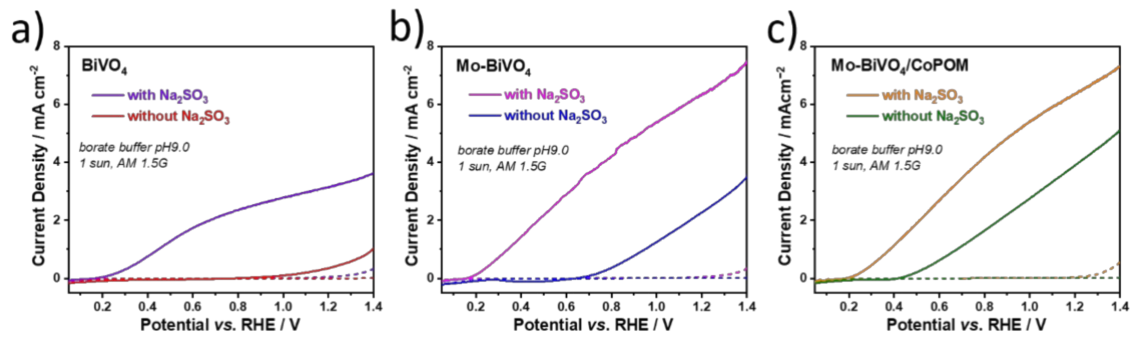


Fig. S18 J-V plots of (a) BiVO₄, (b) Mo-BiVO₄ and (c) Mo-BiVO₄/CoPOM in 0.5 M borate buffer electrolyte pH 9.0 with and without 0.1 M Na₂SO₃ under AM 1.5G one sun illumination. Dotted curves represent measurements in dark.

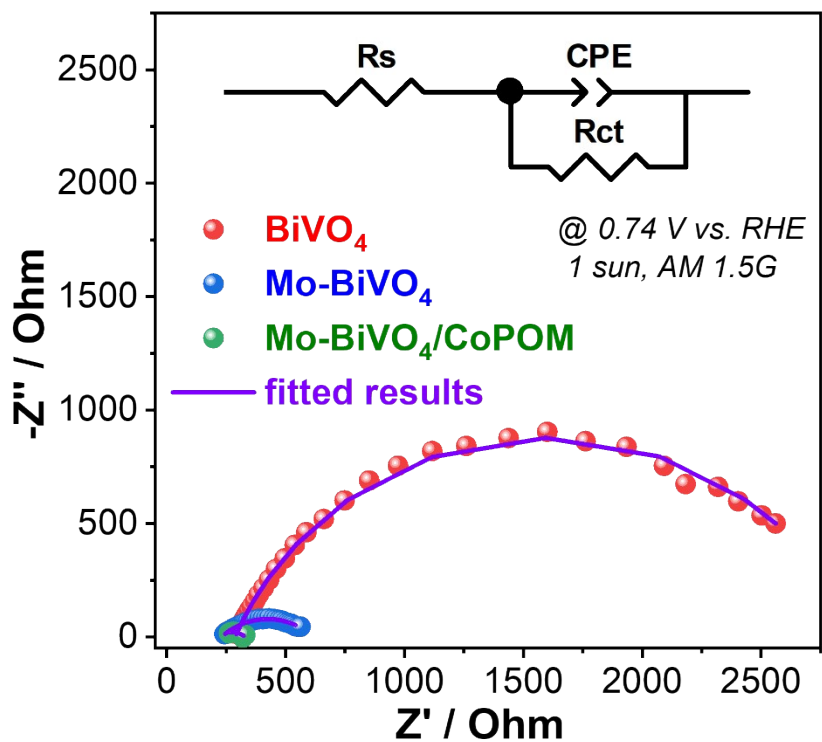


Fig. S19 EIS curves (inset: equivalent circuit used for fitting) of BiVO_4 , Mo-BiVO_4 and $\text{Mo-BiVO}_4/\text{CoPOM}$ in 0.5 M borate buffer electrolyte pH 9.0 under AM 1.5G one sun illumination. Solid curves represent the fitted results.

Tab. S8 The EIS data using circuit in Fig.

| Samples | R_s (Ω) | R_{ct} (Ω) |
|-----------------------------|---|--|
| Mo-BiVO ₄ /CoPOM | 217.3 \pm 11.6 | 113.4 \pm 13.4 |
| Mo-BiVO ₄ | 231.3 \pm 1.5 | 385.3 \pm 6.9 |
| BiVO ₄ | 288.0 \pm 1.9 | 2620.0 \pm 36.5 |

fitted results of the equivalent S19.

References

1. J. Jian, Y. Xu, X. Yang, W. Liu, M. Fu, H. Yu, F. Xu, F. Feng, L. Jia, D. Friedrich, R. van de Krol and H. Wang, *Nat. Commun.*, 2019, **10**, 2609.
2. Q. Yin, J. M. Tan, C. Besson, Y. V. Geletii, D. G. Musaev, A. E. Kuznetsov, Z. Luo, K. I. Hardcastle and C. L. Hill, *Science*, 2010, **328**, 342–345.
3. R. Gong, D. Mitoraj, D. Gao, M. Mundsziinger, D. Sorsche, U. Kaiser, C. Streb, R. Beranek and S. Rau, *Adv. Sustainable Syst.*, 2022, **6**, 2100473.
4. Z. Luo, C. Li, S. Liu, T. Wang and J. Gong, *Chem. Sci.*, 2017, **8**, 91–100.
5. L. Wang, D. Mitoraj, S. Turner, O. V. Khavryuchenko, T. Jacob, R. K. Hocking and R. Beranek, *ACS Catal.*, 2017, **7**, 4759–4767.
6. X. Cao, Y. Wang, J. Lin and Y. Ding, *J. Mater. Chem. A*, 2019, **7**, 6294–6303.
7. H. Dotan, K. Sivula, M. Grätzel, A. Rothschild and S. C. Warren, *Energy Environ. Sci.*, 2011, **4**, 958–964.
8. T. W. Kim and K. Choi, *Science*, 2014, **343**, 990–994.
9. A. W. Sleight, H. Chen and A. Ferretti, *Mat. Res. Bull.*, 1979, **14**, 1571–1581.
10. I. S. Cho, Z. Chen, A. J. Forman, D. R. Kim, P. M. Rao, T. F. Jaramillo and X. Zheng, *Nano Lett.*, 2011, **11**, 4978–4984.
11. S. Bai, S. Jia, S. Yan, Y. Zhao, P. Tang, R. Luo, Y. Feng, D. Li and A. Chen, *Inter. J. Hydrogen Energy*, 2024, **54**, 1008–1016.
12. J. Wang, Y. Zhang, J. Bai, J. Li, C. Zhou, L. Li, C. Xie, T. Zhou, H. Zhu and B. Zhou, *J. Colloid & Interface Sci.*, 2023, **644**, 509–518.
13. P. Yang, H. Shi, H. Wu, D. Yu, L. Huang, Y. Wu, X. Gong, P. Xiao and Y. Zhang, *Nanoscale*, 2023, **15**, 4536–4545.
14. Q. Meng, B. Zhang, H. Yang, C. Liu, Y. Li, A. Kravchenko, X. Sheng, L. Fan, F. Li and L. Sun, *Mater. Adv.*, 2021, **2**, 4323–4332.